



Behaviors and mechanisms of copper adsorption using highly efficient nanostructured superparamagnetic hydroxyapatite

Iraj Kazeminezhad^a, Sana Ahmadizadeh^a, Behrooz Zargar^b, Ali Akbar Babaei^{c,d,*}

^aDepartment of Physics, School of Science, Shahid Chamran University, Ahvaz, Iran, emails: i.kazeminezhad@scu.ac.ir (I. Kazeminezhad), sana.shafiqh@gmail.com (S. Ahmadizadeh)

^bDepartment of Chemistry, School of Science, Shahid Chamran University, Ahvaz, Iran, email: zargar_b@scu.ac.ir

^cEnvironmental Technologies Research Center, Ahvaz Jundishapur University of Medical Sciences, Ahvaz, Iran, Tel. +98 61 33738269; Fax: +98 61 33738282; email: babaei-a@ajums.ac.ir

^dDepartment of Environmental Health Engineering, School of Public Health, Ahvaz Jundishapur University of Medical Sciences, Ahvaz, Iran

Received 28 July 2016; Accepted 16 November 2016

ABSTRACT

A superparamagnetic hydroxyapatite (SPM/Hap) nanocomposite was synthesized to remove Cu²⁺ from aqueous solution. Various factors affecting the uptake behavior such as pH, contact time, initial concentration of Cu²⁺, adsorbent dose, and desorption behavior were studied using batch tests. The results revealed that the adsorption of Cu²⁺ ions was relatively fast and highly pH dependent. The surface complexation mechanism plays a key role for the uptake of Cu²⁺ by SPM/Hap. The pseudo-first-order model showed satisfactory fit with the experimental data. The equilibrium data were well fitted by the Langmuir and Liu isotherm models, with a maximum sorption capacity of 247.6 mg g⁻¹. The results implied that SPM/Hap can be selected as a durable, robust, promising, and environmentally friendly adsorbent for the effective remediation of industrial wastewaters containing heavy metals.

Keywords: Magnetic hydroxyapatite; Copper ion; Nanoparticles; Adsorption; Surface complexation; Mechanisms

1. Introduction

Heavy metals are among the most common environmental pollutants which are usually found in high concentrations in industrial wastewater, posing a risk of damage to the environment and being detrimental to human health [1–3]. Copper is among the most widely applied metals in various industries including electrical, electroplating, pesticide and fertilizer production, wood manufacturing, and pigment industries. The rapid development of these industries and the rampant application of Cu(II)-based herbicides, algicides, and molluscicides in the agricultural sector have led to the accumulation of Cu²⁺ ions in the environment [4–6]. Unlike some pollutants, copper and several other toxic heavy metals are persistent in the environment and are non-biodegradable [7].

High levels of Cu²⁺ ions have been found to result in hepatic, renal and cerebral diseases, kidney damage and anemia, and even possibly leading to death [8,9].

In recent years, a range of conventional treatment technologies have extensively been investigated for the removal of heavy metals and the reduction of their toxic effects. These have included biological methods, membrane processes, electrodialysis, ion exchange, chemical precipitation, and reverse osmosis [10–12]. Many of these methods suffer from disadvantages such as high operating costs, high sludge volume, and the production of secondary pollutants, and are often unfeasible because of their high costs in reducing Cu²⁺ at low concentrations. More recently, there have been some reports on the use of inorganic adsorbents for separating and removing heavy metals from aqueous solutions. Regarding their availability, cost-effectiveness, stability against oxidation and reduction conditions, and the possibility of recycling, inorganic adsorbents are economically viable [13,14].

* Corresponding author.

Traditional inorganic adsorbents with a low surface area lose their ability to absorb. Thus, it seems to be a necessary step to make high capacity adsorbents which serve a fast and easy removal of contaminants. One of the outstanding characteristics of the fast-emerging nanotechnology is the high surface area to volume ratio of nanomaterials [15]. Because of these exceptional features and other unique properties such as high reactivity, nanoparticles are considered as appropriate means to eliminate pollutions in either in situ or ex situ approaches. The application of nanoparticles, compared with other conventional methods, ensures a more cost-effective and a more rapid purification process for wastewater remediation.

Hydroxyapatite, with the chemical formula of $\text{Ca}_{10}(\text{PO}_4)_6(\text{OH})_2$, Hap as its symbol, and the most important member of the calcium phosphate family, is not only the major mineral in the composition of the bone, dentin, and enamel, but it also has a wide range of applications in the medical field [16]. Besides, other characteristics of hydroxyapatite such as the ability to incorporate a variety of heavy metals into its crystal structure, its high biocompatibility and very low solubility in water as well as its high stability against oxidation and reduction conditions make it a prominent adsorbent to be used in remediation of all types of industrial wastewater contaminated with heavy metals. Applications of Hap as a powerful material for the adsorption of heavy metals have widely been reported in previous studies [16,17]. However, in case of this strong adsorbent, the common drawback is the inconvenience to separate it after adsorption by the pollutant.

In this regard, magnetic separation technology is a new methodology used as a simple, fast, efficient, and economical method for the separation and preconcentration of environmental contaminants. Other advantages of this method include the large active surface area and the high adsorption capacity, as well as the ability to process a solution containing suspended solids hence producing less secondary waste [18,19]. In addition, magnetite can be easily separated by an external magnetic field. This extraordinary advantage is especially useful for the recovery or reuse of the magnetic nanoparticles [18,19].

Although studies on environmental clean-up by means of magnetic hydroxyapatite have been conducted in recent years, but they are limited [20] and further studies are needed to lead to an effective application of the adsorbent in cleaning up the environment. Therefore, the superparamagnetic hydroxyapatite (SPM/Hap) nanocomposite adsorbent was synthesized (by co-precipitation), characterized, and used as the adsorbent material for removing Cu^{2+} ions from aqueous solutions. First, the optimum adsorption conditions were determined as a function of the solution's pH, the contact time, the initial concentration of Cu^{2+} , and the adsorbent dosage. Further, isotherms and kinetics were investigated, and the adsorption capacity of SPM/Hap to Cu^{2+} was evaluated.

2. Materials and methods

2.1. Materials

$\text{FeCl}_2 \cdot 4\text{H}_2\text{O}$, $\text{FeCl}_3 \cdot 6\text{H}_2\text{O}$, NH_4OH (25%), $\text{Ca}(\text{NO}_3)_2 \cdot 4\text{H}_2\text{O}$, $(\text{NH}_4)_2\text{HPO}_4$, and ethylenediaminetetraacetic acid (EDTA) were purchased from Merck, Germany. All solutions for the

metal adsorption experiments were prepared using their nitrate salts. Deionized water was used throughout all the experiments. All other chemicals were of analytical grade and were used without further purification.

2.2. Synthesis and characterization of SPM/Hap

In this study, the SPM/Hap nanocomposite was synthesized by co-precipitation method according to Feng et al.'s study [21] with some modification. First, iron salts of Fe(III) and Fe(II) (in a 2:1 molar ratio) were dissolved in 30 mL of deoxygenated water under nitrogen atmosphere at room temperature, and then 10 mL of 25% NH_4OH solution was added to the ferrous solution under N_2 with vigorous mechanical stirring (500 rpm) for 15 min, producing iron oxide dark solids immediately. A suspension of Fe_3O_4 (2.1 wt%) was added to the mixture solution of $\text{Ca}(\text{NO}_3)_2$ with $(\text{NH}_4)_2\text{HPO}_4$ in a molar ratio of 5:3 (the whole Ca/P mole ratio of the mixture was 1.67). After mechanical stirring for 30 min, 25% NH_4OH solution was added to the mixture while the pH was kept above 11.0. The resulting dark brown suspension was heated at 110°C for 2 h and then the mixture was cooled to room temperature and kept for 24 h in stagnant. The obtained magnetic Hap composite adsorbent was separated by an external magnetic field and washed repeatedly with deionized water until the pH was neutral. The dried composite particles were obtained after the products were dried for 24 h in a vacuum drying oven. Then the dark brown magnetic powder was calcined at 200°C in order to increase the porosity and specific surface area of the adsorbent. The resulting products were the SPM/Hap adsorbents. Physicochemical features of the SPM/Hap nanoparticles are listed in Table 1.

The adsorbent SPM/Hap was characterized using a X-ray diffractometer (XRD; Model PW 1830/40, Philips, Germany) with $\text{CuK}\alpha$ ($\lambda = 1.5418 \text{ \AA}$) incident radiation over the 2θ range of 10° – 80° at room temperature with a step size of 0.02° . The size and morphology of SPM/Hap were investigated by the field emission scanning electron microscopy (FESEM; Model VEGAII, XMU, Tescan, Czech Republic). To study the chemical structure of the samples, Fourier transform infrared spectroscopy (FTIR; Model Bomem/MB102, ABB Company, Switzerland) was used. To this end, the samples prepared from 1:80 Hap–KBr mixtures (by weight) were compacted into pellet form and then scanned from 4,000 to 400 cm^{-1} . The magnetization measurements were performed at room temperature using a vibrating sample magnetometer (VSM).

Table 1
Physicochemical properties of SPM/Hap nanoparticles

Parameters	Values
Brunauer–Emmett–Teller surface area ($\text{m}^2 \text{ g}^{-1}$)	372.5
Ca (wt%)	25.4
P (wt%)	11.9
Hap content (wt%)	63.7
Ca/P molar ratio	1.67
pH_{zpc}	6.5 ± 0.2
Particle size (nm)	19 ± 2

2.3. Adsorption of Cu²⁺ experiments

Laboratory batch experiments were carried out to study the adsorption behavior of the SPM/Hap for Cu²⁺ ions at room temperature (25°C ± 1°C) using 150 mL Erlenmeyer flasks containing 50 mL of Cu²⁺ solution. An appropriate amount of SPM/Hap was added to 50 mL of the corresponding Cu²⁺ solution over a period of time on a shaker at 150 rpm. After the adsorbent was separated magnetically, the quantitative analysis of Cu²⁺ in an aqueous solution was performed using a flame atomic absorption spectrometer (Vario 6, Analytik Jena, Germany). In this study, the effect of various parameters such as the solution's pH, the amount of adsorbent, the initial concentration of the Cu²⁺, and the contact time were investigated. All the experiments were performed in triplicate and the averaged values were recorded. For the experiment of pH effect, the adsorption of Cu²⁺ by SPM/Hap was investigated at the pH range of 2.0–8.0. The initial pH of the solution was adjusted by using 0.1 M HNO₃ and 0.1 M NaOH. Except for the experiment of pH effect, the pH of all the original solution was controlled at 5.0–6.0. The initial Cu²⁺ concentration of 10 mg L⁻¹ was used for the adsorption experiments considering the low concentration (0–10 mg L⁻¹) of heavy metals in natural water. Adsorption isotherm studies were conducted by 0.0015–0.1 g SPM/Hap with 50 mL Cu²⁺ solution containing 10 mg L⁻¹ Cu²⁺ in 150 mL Erlenmeyer flasks. To achieve the saturated adsorption, the sample solution was shaken for 1 h at 150 rpm and 25°C ± 1°C, and then the concentrations of the metal ions were analyzed.

Adsorption kinetic experiments were carried out by the batch adsorption method at 25°C ± 1°C. A series of samples were prepared by mixing Cu²⁺ solution (50 mL, 10 mg L⁻¹) with 0.05 g SPM/Hap in 150 mL Erlenmeyer flasks. Samples were withdrawn from the shaker at different time intervals (1–120 min) and analyzed for the determination of metal ion concentrations. The feasibility of the applied adsorbent was examined through the adsorptive reaction with Cu(II) in the acid mine drainage (AMD) of Sarcheshmeh Copper Complex (Kerman, Iran). The basic features of AMD are reported in Supplementary Table 1.

The adsorption capacity (q_e) and the removal efficiency (R) of Cu²⁺ were obtained via the following equations:

$$q_e = \frac{(C_o - C_e)V}{m} \quad (1)$$

$$R = \frac{C_o - C_e}{C_o} \times 100 \quad (2)$$

where q_e (mg g⁻¹) is the amount of Cu²⁺ ions adsorbed onto the unit amount of the adsorbent, C_o and C_e (mg L⁻¹) are the initial and equilibrium Cu²⁺ ion concentrations, respectively, V (L) is the volume of the solution, and m (g) is the adsorbent mass in dry form.

During the desorption and reuse study, appropriate SPM/Hap was set into the 150 mL Erlenmeyer flasks containing metal ion solutions (50 mL, 10 mg L⁻¹). They were then shaken severely using a horizontal shaker for approximately 2 h. In the next step, the SPM/Hap samples loaded with metal ions were separated magnetically and cleansed sequentially via both distilled and deionized

water several times in order to eliminate the concentration of unattached metal ions. The removal efficiency of ions was determined using an atomic absorption spectrometry instrument and was calculated according to Eq. (2). In the desorption experiments, the reacted adsorbents with the adsorbate were mixed in 100 mL of EDTA solutions (0.05 M) at pH 3.0 and 5.0, followed by five sequential sorption/desorption cycles.

2.4. Adsorption isotherm and kinetic models

With regard to the adsorptive remediation of water and wastewater containing contaminants such as heavy metals, it is essential to know the removal rate for the design and the quantitative evaluation of the adsorbent. In addition, the kinetics describes the adsorbate uptake rate which controls the residence time of the adsorbate uptake at the adsorbent–solution interface. Therefore, it is important to be able to predict the metallic ion uptake removal rate from aqueous solutions in order to design an appropriate adsorption unit.

To determine the parameters of the isotherm and kinetic models, the Cu²⁺ adsorption data were fitted to the non-linear kinetic and isotherm models using MATLAB® 7.11.0 (R2010b), with successive interactions calculated by the Levenberg–Marquardt algorithm. Since the unwanted falsification of error distribution occurs due to data transformation to a linear form, the nonlinear method is superior to the linear one in determining the parameters of the isotherm and kinetic models [19,22].

In this study, four widely used adsorption isotherm models (Langmuir, Freundlich, Redlich–Peterson, and Liu) and six general adsorption kinetic models (pseudo-first-order equation of Lagergren, pseudo-second-order equation of Ho, Elovich, fractional power function, Avrami fractional order, and intraparticle diffusion model) were used to describe the adsorption equilibrium and the adsorption kinetics of Cu²⁺ onto SPM/Hap nanoparticles, respectively [18]. All the used mathematical isotherm and kinetic models have been summarized in Supplementary Table 2.

2.5. Models fitness

To select of the most suitable kinetic and isotherm model, it is necessary to evaluate their validity. Here, the validity of the kinetic and isotherm models were assessed by such criteria as the determination coefficient (R^2), the adjusted determination coefficient (R^2_{adj}), the sum squared error (SSE), and the root mean square error (RMSE) [18,23]. These criteria describe the goodness of fit between the experimental and predicted data. The best model was chosen based on the lowest RMSE and SSE, as well as with R^2_{adj} and R^2 as close as possible to one. R^2 , R^2_{adj} , SSE, and RMSE can be calculated according to Supplementary Table 3.

3. Results and discussion

3.1. Adsorbent characterization

Fig. 1(a) shows the X-ray diffraction pattern of the SPM/Hap adsorbent. There are five characteristic peaks for Hap ($2\theta = 25.87^\circ, 31.74^\circ, 39.75^\circ, 46.61^\circ, \text{ and } 49.47^\circ$) and four for

Table 2

Kinetic parameters for Cu²⁺ adsorption using SPM/Hap adsorbent (conditions: pH 5.5 ± 0.1, adsorbent dose 1.0 g L⁻¹, Cu²⁺ 10 mg L⁻¹, 25°C ± 1°C)

Adsorption kinetic models	Parameters (unit)	Values	R ² _{adj}	RMSE	SSE
Pseudo-first-order (Lagergren)	k_f (min ⁻¹)	2.085	0.9999	0.03546	0.01006
	$q_t = q_e(1 - \exp(-k_f t))$	q_e (mg g ⁻¹)	9.99		
Pseudo-second-order (Ho)	k_s (g mg ⁻¹ min ⁻¹)	0.78	0.9982	0.1318	0.1389
	$q_t = \frac{k_s q_e^2 t}{1 + q_e k_s t}$	q_e (mg g ⁻¹)	10.09		
Elovich	α (mg g ⁻¹ min ⁻¹)	18,230	0.8708	1.126	10.14
	$q_t = \left(\frac{1}{\beta}\right) \ln(1 + \alpha\beta t)$	β (g mg ⁻¹)	1.33		
Avrami fractional order	k_{AV} (min ⁻¹)	6.08	0.9806	0.436	1.33
	$q_t = q_e \left\{ 1 - \exp[-(k_{AV} t)^{n_{AV}}] \right\}$	q_e (mg g ⁻¹)	9.83		
		n_{AV}	5.74		
Fractional power function	a (mg g ⁻¹ min ^{-b})	9.42	0.9906	0.303	0.7346
	$q_t = at^b$	b	0.015		
Intraparticle diffusion	k_{id} (mg g ⁻¹ min ^{-0.5})	0.306	0.08951	2.989	71.49
	$q_t = k_{id} t^{\frac{1}{2}} + C$	C	7.342		

Table 3

Isotherm parameters for Cu²⁺ adsorption using SPM/Hap adsorbent (conditions: pH 5.5 ± 0.1, adsorbent dose 0.03–2.0 g L⁻¹, Cu²⁺ 10 mg L⁻¹, 25°C ± 1°C)

Adsorption isotherm models	Parameters (unit)	Values	R ² _{adj}	RMSE	SSE
Langmuir	q_m (mg g ⁻¹)	247.6	0.996	5.3	224.6
	$q_e = \frac{K_L q_m C_e}{1 + K_L C_e}$	K_L (L mg ⁻¹)	2.87		
Freundlich	K_F (mg g ⁻¹)	159	0.93	22.06	3,894
	$q_e = K_F C_e^{\frac{1}{n}}$	(mg L ⁻¹) ⁻ⁿ			
		n	2.664		
Redlich–Peterson	K_{RP} (L g ⁻¹)	698.3	0.995	5.65	223.3
	$q_e = \frac{K_{RP} C_e}{1 + a_{RP} C_e^g}$	a_{RP} (L mg ⁻¹)	2.792		
		g (0 < g < 1)	1.009		
Liu	q_m (mg g ⁻¹)	243.0	0.996	5.54	214.9
	$q_e = \frac{q_m (K_s C_e)^{n_L}}{1 + (K_s C_e)^{n_L}}$	K_s (L mg ⁻¹)	3.018		
		n_L	1.045		

Fe₂O₃ (2θ = 35.43°, 53.67°, 56.94°, and 62.53°). This pattern indicates that the diffraction peaks (0566-074-01 ICSD) and (00-013-0458 ICDD) are in agreement with the standard card of hexagonal hydroxyapatite (P63/m) and the tetragonal structure of γ-Fe₂O₃, respectively.

Magnetization of the synthesized SPM/Hap nanocomposite was studied in the range of ±10,000 Oe using a VSM. As shown in Fig. 1(b), the saturation magnetization (Ms) and the coercive force (Hc) were estimated to be 2.83 emu g⁻¹

and 0 Oe, respectively. These magnetic properties are lower than bulk γ-Fe₂O₃ particles (Ms = 74 emu g⁻¹ and Hc = 500–800 Oe) but they are almost in accordance with previous reports [24]. As can be seen from Fig. 1(b), the remanence of the synthesized SPM/Hap is almost zero, demonstrating the superparamagnetic behavior of the nanocomposite. This behavior prevents SPM/Hap nanoparticles from aggregation, enabling them to redisperse rapidly when the magnetic field is removed [24] and allowing the magnetic separation

of SPM/Hap by the application of an external magnetic field within a short time.

SEM image in Fig. 1(c) shows the morphology and the particle size of magnetic nanoparticles. As seen in the figure, the prepared nanoparticles are almost spherical in shape and loosely agglomerated. The agglomeration of the particles may be due to the decreased particle size as well as the increased surface energy of the particle. Mean particle size of SPM/Hap is 19 ± 2 nm. Because of the superparamagnetic properties of the SPM/Hap, this nanoparticle has a broad range of applications in industrial catalysis, environmental protection, biomedicine, and bioengineering in all of which it prevents particle agglomeration and enables the particles to redisperse rapidly when the magnetic field is removed.

FTIR was done to confirm the formation of the bonds in SPM/Hap structure. Fig. 1(d) shows the FTIR spectrum of the SPM/Hap nanoparticles. The adsorption band at 566 cm^{-1} can be referred to as the bending modes of the bonds in the phosphate group. The apparent band at around $1,022\text{--}1,100 \text{ cm}^{-1}$ is attributed to the O–P–O asymmetrical stretching in the phosphate group. The broadband at around $3,000$ and $3,500 \text{ cm}^{-1}$ is assigned to the hydroxyl group bending mode. The FTIR studies show that the required bonds have been formed in sample structures.

3.2. Cu^{2+} adsorption

3.2.1. Effect of solution pH and copper removal mechanism

The aqueous solution's pH plays a key role in the adsorption processes of heavy metals. The effect of pH on the adsorption of Cu^{2+} by SPM/Hap nanoparticles is shown in Fig. 2. A maximum Cu^{2+} removal was observed at pH 5.0–6.0 and a decline in the adsorption capacity was observed in acidic conditions. The removal efficiency by SPM/Hap increased from 65.4% to 98.0% with an increase in pH from 2.0 to 6.0. However, the removal efficiency remains almost constant at higher pH values.

The most possible reason for justification of this phenomenon is principally rooted in two common reactions which

are, in essence, able to remove Cu^{2+} from aqueous solutions. Initially, the most effective mechanism involved in the adsorption of Cu^{2+} onto the adsorbent is the so-called surface complexation of SPM/Hap which has a robust correlation with the changes of pH values in the solution. Surface complexation reaction can be explained as follows:



In low initial pH values range (i.e., below $\text{pH}_{\text{ZPC}} = 6.5$), the protonation of surface $\equiv\text{PO}^-$ and $\equiv\text{CaOH}^0$ groups led to the dropping of the amount of protons, which resulted in an increase in the final pH values (see Fig. 2). These results are confirmed by other studies on the sorption of heavy metals on hydroxyapatite [20,25]. Moreover, the existence of $\equiv\text{CaOH}_2^+$ and neutral $\equiv\text{POH}^0$ sites with apparently positive charges brought about the creation of such positive regions in the corresponding pH values. Thus, the lower adsorption of Cu^{2+} at lower pH values can be ascribed to the increase of positive surface charge on SPM/Hap with decreasing solution pH, which created an unfavorable surface complexation of the Cu^{2+} on the adsorbent surface compared with the net negative charge sites. As a result, the removal efficiency of Cu^{2+} obviously declined in pH values less than 3.0 (Fig. 2). In addition, the smaller adsorption capabilities of SPM/Hap at lower pH levels are probably due to the significant competition between Cu^{2+} and hydrogen ions for the adsorption sites [26,27]. Moreover, another reason for a decrease in Cu^{2+} removal efficiency in acidic pH conditions would be ascribed to the promotion of the dissolution of Hap nanoparticles. In this regards, we observed that the adsorbent dosage was decreased in such acidic pH values.

For a better understanding of the mechanism of Cu^{2+} adsorption on SPM/Hap, the pH variation before and after adsorption as well as the Cu^{2+} and Ca^{2+} ion concentrations were monitored in a series of experiments with different initial concentrations of Cu^{2+} (Fig. 3). Moreover, blank tests

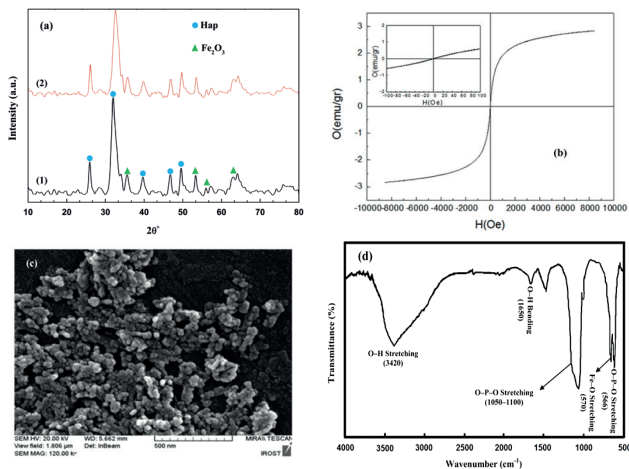


Fig. 1. (a) X-ray diffractogram (SPM/Hap (1) Cu^{2+} -loaded SPM/Hap (2)), (b) magnetization curve, (c) SEM image, and (d) FTIR spectra of the prepared SPM/Hap nanocomposite.

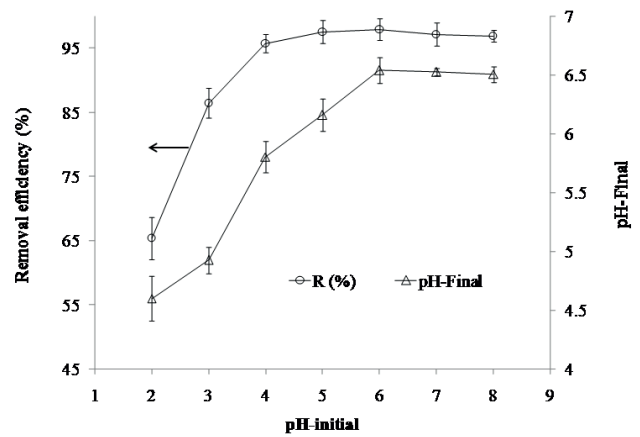


Fig. 2. Relationship between initial pH and final pH value obtained after equilibration of SPM/Hap with Cu^{2+} solution and the copper removal efficiency by SPM/Hap adsorbent (contact time 60 min, adsorbent dose 0.25 g L^{-1} , Cu^{2+} 10 mg L^{-1} , $25^\circ\text{C} \pm 1^\circ\text{C}$).

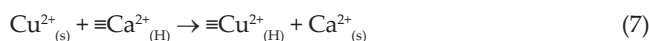
were performed by mixing the SPM/Hap composite with an aqueous solution without Cu^{2+} ions at pH 5.0. The final pH value of the solution was approximately the same as at the beginning and equal to the zero point charge (pH_{ZPC}) (6.5) of the adsorbent due to the buffer capacity of SPM/Hap.

pH_{ZPC} is defined as the pH value of the suspension, at which the protonic net surface charge is equal to zero. Since the pH_{ZPC} of SPM/Hap is 6.5, the surface of the SPM/Hap is positively charged at pH 5.0, which is unfavorable for Cu^{2+} uptake. Therefore, adsorption of Cu^{2+} onto the adsorbent in this pH range is unexplainable by the electrostatic attraction mechanism. The significant difference between the amount of Cu^{2+} uptaken and Ca^{2+} released (see Fig. 3) indicates that adsorption mechanisms other than ion exchange and dissolution-precipitation may play a key role for the uptake of Cu^{2+} . As shown in Fig. 3, the final pH value dropped as

the uptaken Cu^{2+} ions increased. The total quantities of the displaced H^+ are equivalent to the amount of metal ions disappearing from the solution. The pH decline in equilibrium indicates that H^+ ions are liberated from the surface $\equiv\text{POH}$ sites of SPM/Hap into the solution as a result of being replaced with Cu^{2+} according to the following reactions, which, to some extent, confirms the contribution of surface complexes to the overall sorption mechanism [20,28].



Secondly, ion-exchange reaction between the adsorbed Cu^{2+} and Ca^{2+} of SPM/Hap is assumed to be the next likely cause of Cu^{2+} removal. The ion-exchange reaction can be expressed via the following equation:



where subscripts (s) and (H) denote solution and SPM/Hap phases, respectively. The metal in the solution ($\text{Cu}^{2+}_{(s)}$) replaces a surface Ca^{2+} of the adsorbent ($\equiv\text{Ca}^{2+}_{(H)}$). Therefore, the acidic pH values, primarily leading to their undeniable role on the enhancement of Cu^{2+} concentration in aqueous solutions and inhibiting the ion exchange of Cu^{2+} with Ca^{2+} of the adsorbent, can significantly decline the adsorption of Cu^{2+} onto the surface of SPM/Hap. According to other reports, the Ca^{2+} ions in hydroxyapatite can be easily ion exchanged with many other metal ions [20,25]. The ionic radius of Cu^{2+} (0.073 nm) is significantly smaller than that of Ca^{2+} (0.099 nm). It is reasonable, therefore, that Ca^{2+} ions can be easily substituted in the HAP crystal lattice. Fig. 1(a)(2) presents the XRD patterns of Cu^{2+} -loaded SPM/Hap. Phase analyses of the solid residue with maximum uptake capacity of Cu^{2+} after exposure to a 100 mg L^{-1} Cu^{2+} solution showed neither the structural changes of nano-SPM/Hap nor the shift of the SPM/Hap peaks in XRD which is possibly the result of an ion exchange in the SPM/Hap structure [25]. Conversely, the crystallite size of SPM/Hap was calculated based on the peak broadening of the XRD diagram through Scherrer's formula as follows [29,30]:

$$D_{hkl} = \frac{k\lambda}{\beta_{1/2} \cos\theta_{hkl}} \quad (8)$$

where k is defined as a dimensionless constant which is different with actual shape of crystallite and is selected to be 0.9 for elongated Hap crystallites, λ is the $\text{CuK}\alpha$ radiation ($\lambda = 0.15418 \text{ nm}$) wavelength, $\beta_{1/2}$ corresponds to full width at half maximum (FWHM) for the peak hkl (rad) and θ_{hkl} is Bragg angle (in degree). The line broadening of the (211) ($2\theta = 31.74$) reflection was applied to determine the mean crystal size.

The degree of crystallinity, X_c , can be expressed as the fraction of the crystalline phase in a sample volume. The equation below describes a practical relationship between X_c and $\beta_{1/2}$ as follows:

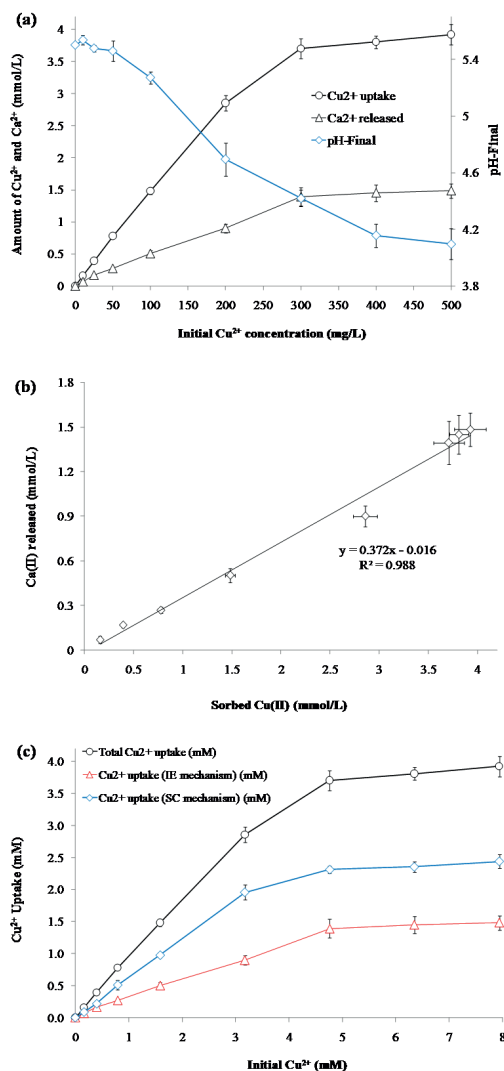


Fig. 3. (a) Adsorbed Cu^{2+} , released Ca^{2+} , and final value of solution pH at different initial concentration of Cu^{2+} , (b) adsorbed Cu^{2+} against released Ca^{2+} , and (c) adsorbed Cu^{2+} via surface complexation (SC) and ion-exchange (IE) mechanisms (reaction time 60 min, adsorbent dose 1.0 g L^{-1} , initial solution $\text{pH} 5.5 \pm 0.1$, $25^\circ\text{C} \pm 1^\circ\text{C}$).

$$X_c = \left(\frac{K_A}{\beta_{1/2}} \right)^3 \quad (9)$$

where K_A is a constant set at 0.24 and $\beta_{1/2}$ is the FWHM of the (211) reflection (in degree). The crystallite size for SPM/Hap and Cu²⁺-loaded SPM/Hap obtained at 5.62 and 4.72 nm, respectively. Additionally, the crystallinity degree of SPM/Hap and Cu²⁺-loaded SPM/Hap was 0.0044 and 0.0025, respectively. The decrease in the values of crystallinity and crystallite size of SPM/Hap was observed after copper adsorption. The most probable proof of this evidence is an inconformity between the ion size of Cu²⁺ and Ca²⁺. Since the radius of Cu²⁺ ions (0.072 nm) differ from radius of Ca²⁺ (0.099 nm), it will distort the crystallinity of SPM/Hap [48]. The obtained results confirm ion-exchange mechanism [25]. The results of present study quite match with Miyaji et al.'s research [31] who found an indirect relationship between crystallinity and increase in Zn concentration. In similar research, Meski et al. [25] reported a sharp reduction in the crystallinity and crystallite size of Hap with Zn²⁺ adsorption.

To prove this assumption, Ca²⁺ ion concentration was monitored in a series of experiments with different initial concentrations of Cu²⁺ to verify whether the Ca²⁺ was released in the solution after the equilibrium adsorption process. As shown in Fig. 3(a), the concentration of Ca²⁺ in the solution increased significantly after Cu²⁺ adsorption (from 6.24 to 69.33 and 6.99 to 1,483 $\mu\text{mol L}^{-1}$ for 10 and 500 mg L⁻¹ Cu²⁺ solutions, respectively). Additionally, Fig. 3(b) shows a linear relationship between sorbed Cu²⁺ and released Ca²⁺ with significantly high coefficient of determination ($R^2 = 0.988$).

Thus, it can be concluded that there was also an ion-exchange mechanism in the adsorption process of Cu²⁺ by SPM/Hap in addition to surface complexation [21]. However, based on the findings of batch experiments, the ion exchange was not the dominant mechanism in the process of Cu²⁺ adsorption. According to Fig. 3(c), the influence of ion exchange was relatively half of the surface complexation pattern on the adsorption of Cu²⁺ in aqueous solution.

Even though it is likely that part of the released Ca²⁺ in the solution is due to dissolution and precipitation mechanisms by the formation of a copper-containing hydroxyapatite, given the lack of any structural changes of nano-SPM/Hap peaks in XRD after exposure to a 100 mg L⁻¹ Cu²⁺ solution with maximum uptake capacity of Cu²⁺, it is suggested that the dissolution-precipitation mechanism probably does not play a role in the removal of copper.

The high removal efficiency of Cu²⁺ at pH values higher than 6.0 may be attributable to the precipitation of Cu(OH)₂ rather than the adsorption of Cu²⁺ by SPM/Hap. Therefore, the optimum pH for Cu²⁺ ion sorption is found in the pH range of 5.0–6.0, which is in accordance with previous reports [26,29]. Further experiments performed at pH 5.5 confirm that SPM/Hap is an efficient adsorption material for the removal of Cu²⁺ from natural water.

3.2.2. Effect of adsorbent dosage

SPM/Hap adsorbent doses of 0.03–2.0 g L⁻¹ were evaluated to determine the effect of dosage on the adsorption capacity. Fig. 4 shows the effect of adsorbent dosage on

the removal of Cu²⁺. The Cu²⁺ removal efficiency increased from 66.8% to 99.3% with the increase in SPM/Hap dosage from 0.03 to 0.25 g L⁻¹ (Fig. 4). No further increases in Cu²⁺ removal efficiency were observed at any dosage greater than 0.25 g L⁻¹. Thus, 0.25 g L⁻¹ was determined to be the optimal adsorbent dose for Cu²⁺ removal with SPM/Hap. The increase in the adsorption as a result of increasing the adsorbent dose may be attributable to the increase of available active sites and a higher surface area available at higher adsorbent dose for a constant initial value of Cu²⁺ concentration. However, too high adsorbent dose can cause aggregation of adsorbent, resulting in a decrease of the total surface area of the adsorbent and the availability of active sites [7].

3.2.3. Effect of contact time and adsorption kinetics

The adsorption of Cu²⁺ on SPM/Hap was also studied as a function of contact time in order to find out the equilibrium time for maximum adsorption. Fig. 5 shows the adsorption capacity and the percentage removal of Cu²⁺ for initial concentration of 10 mg L⁻¹ by SPM/Hap (1.0 g L⁻¹). The initial adsorption rate of Cu²⁺ onto SPM/Hap was rapid, reaching equilibrium at 5 min (Fig. 5). The maximum adsorption occurred at the first 5 min, and then the sorption rate reached a constant value, which is probably due to plentiful sorption sites and large surface area available for the adsorption of Cu²⁺ on SPM/Hap. This may as well be attributed to the external surface adsorption. Thus, 5 min was determined as the optimal contact time for Cu²⁺ adsorption onto SPM/Hap. In the subsequent experiments, the contact time of 30 min was chosen to ensure reaching equilibrium. This indicates that a significant part of the adsorption sites of the adsorbent exist in the exterior of the SPM/Hap nanoparticles and are easily accessible by Cu²⁺ species, thus resulting in a rapid approach to equilibrium.

Kinetics describes solute uptake rates and defines the residence time of the adsorbate at the solid-liquid interface as well. Additionally, valuable insights into the reaction pathways and the adsorption mechanisms can be achieved via kinetic studies. Kinetic experiments were performed using the SPM/Hap dosage, the solution pH, and the initial Cu²⁺

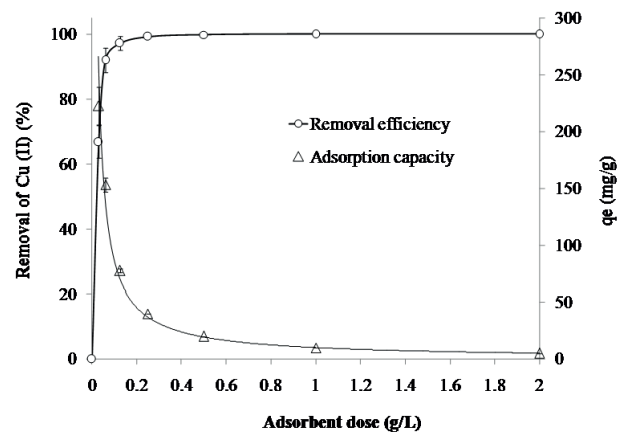


Fig. 4. Effect of adsorbent dosage on the adsorption of Cu²⁺ by SPM/Hap (contact time 60 min, pH 5.5 ± 0.1, Cu²⁺ 10 mg L⁻¹, 25°C ± 1°C).

concentration of 1.0 g L^{-1} , 5.5 and 10 mg L^{-1} , respectively, at $25^\circ\text{C} \pm 1^\circ\text{C}$ (Fig. 5).

As shown in Fig. 5, Cu^{2+} uptake seemed to occur in two steps. The first step involved extremely fast metal uptake within the first 2 min of contact followed by the subsequent removal of Cu^{2+} , which continued for a relatively short period of time until adsorption equilibrium was obtained. The fitting plots using six kinetic equations are shown in Fig. 6, which were simulated with 99% confidence bounds using non-linear equations of pseudo-first-order, pseudo-second-order, fractional power function, Elovich, Avrami fractional order, and Weber–Morris intraparticle diffusion kinetic models. The kinetic parameters acquired from non-linear fitting results are presented in Table 2. Based on the higher values of the adjusted determination coefficient ($R^2_{\text{adj}} > 0.99$) and the lower values of the $\text{SSE} < 1.0$ and the $\text{RMSE} < 1.0$, it can be concluded that the kinetic models of pseudo-first-order, pseudo-second-order, and fractional power function kinetic models were the most appropriate to represent the Cu^{2+} adsorption onto SPM/Hap nanoparticles. Also, the

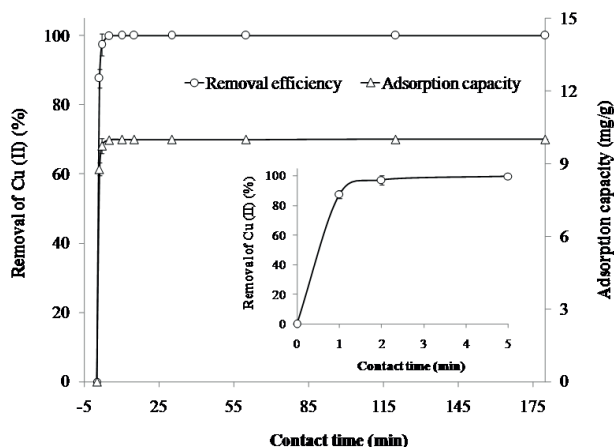


Fig. 5. Effect of contact time on the Cu^{2+} ions adsorption onto SPM/Hap (adsorbent dose 1.0 g L^{-1} , $\text{pH } 5.5 \pm 0.1$, $\text{Cu}^{2+} 10 \text{ mg L}^{-1}$, $25^\circ\text{C} \pm 1^\circ\text{C}$).

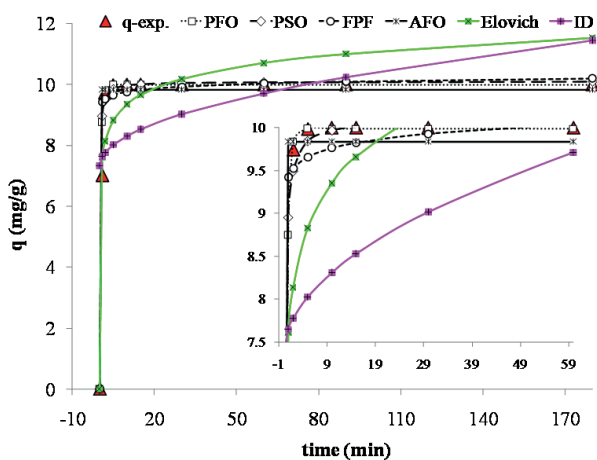


Fig. 6. Non-linear adsorption kinetics curves of Cu^{2+} by SPM/Hap adsorbent ($\text{pH } 5.5 \pm 0.1$, adsorbent dose 1.0 g L^{-1} , $\text{Cu}^{2+} 10 \text{ mg L}^{-1}$, $25^\circ\text{C} \pm 1^\circ\text{C}$).

calculated equilibrium adsorption capacity (q_{cal}) for the pseudo-first-order and pseudo-second-order kinetic models (9.99 and 10.09 mg g^{-1} , respectively) were well approximated to the experimental value (q_{exp}) (10 mg g^{-1}), indicating better suitability of these kinetic models to describe adsorption kinetics of Cu^{2+} onto SPM/Hap. Nonetheless, the highest R^2_{adj} and lowest RMSE and SSE values for the pseudo-first-order kinetic model in Table 2 suggest this model can be used to represent the kinetic uptake of Cu^{2+} onto SPM/Hap.

Our results, however, are somewhat inconsistent with other studies. According to other reports [4,7], the adsorption of the Cu^{2+} ions on different used adsorbents follows the pseudo-second-order kinetic reaction better than the pseudo-first-order one. However, all of these studies have employed linear models instead of nonlinear ones. In the case of pseudo-second-order kinetics, the results from the five linear equations of pseudo-second-order kinetic model were entirely different (data not shown). Also, the fact that the best and the worst fit of experimental kinetic data in pseudo-first-order kinetics was achieved via using non-linear and linear equations, respectively, suggests the kinetics is transforming to the worse while linearizing the non-linear kinetic equations (linear data not shown). Over the past decades, the linear least squares method to the linearly transformed kinetic equations has been developed as a major option for the prediction of optimum kinetic and the evaluation of the model parameters. However, recent investigations have indicated that the unwanted falsification of error distribution occurs due to data transformation to a linear form. Therefore, the nonlinear approach is superior to the linear one for estimating the adsorption kinetic parameters [22].

3.3. Adsorption isotherms

The adsorption isotherms are usually considered as feasible tools to understand the adsorption process. In this work, experimental data were fitted to four widely used isotherm models; namely, Langmuir, Freundlich, Redlich–Peterson, and Liu using non-linear equations (see Fig. 7). The parameters obtained from the studied isotherms are given in Table 3.

The high adjusted correlation coefficient (R^2_{adj}) and the low RMSE and SSE values indicated that the experimental data fitted satisfactorily the Liu, Langmuir, and Redlich–Peterson (R–P) models. Although based on the R^2_{adj} , RMSE, and SSE, the Redlich–Peterson (R–P) model was among the best isotherm models for Cu^{2+} adsorption by SPM/Hap adsorbent, the fact is that since g is greater than 1, this isotherm model is invalid. Both Liu and Langmuir models showed (Table 3) the highest R^2_{adj} and lowest RMSE and SSE values, which means that the q fit by the isotherm model was close to the q measured experimentally. The Langmuir model assumes that the sorption of metal ions onto the surfaces of the adsorbent happens through a monolayer adsorption on a homogeneous surface without mutual action between the adsorbed and the free metal ions [32]. The Liu isotherm model, in addition, is intrinsically a mixture of both the Freundlich and Langmuir models where the concepts of monolayer adsorption hypothesis of Langmuir and adsorption of metal ions onto the heterogeneous surfaces of adsorbents, which are specifically rooted in the Freundlich model, were relatively adjusted. Based on the Liu model assumptions, all reactive sites onto

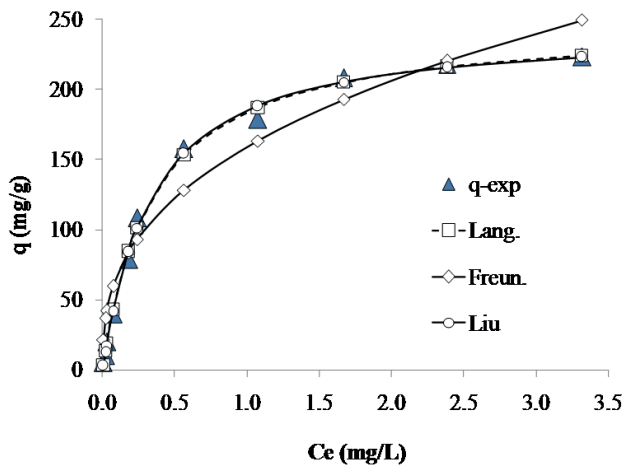


Fig. 7. Non-linear fit of experimental data obtained using Langmuir, Freundlich, and Liu isotherm models.

the surfaces of the adsorbent have no similar energy. Hence, the adsorbent would have several reactive sites that tend to be occupied with the adsorbate molecules [33]. Considering various functional groups on the SPM/Hap, our results show that the active sites of the SPM/Hap will not naturally be able to share the same amount of energy.

Based on the Liu and Langmuir models, the maximum amount of Cu^{2+} uptake by SPM/Hap adsorbent were 243.0 and 247.6 mg g^{-1} , respectively. These values indicate that SPM/Hap is a unique adsorbent for Cu^{2+} removal from aqueous solutions. In the Langmuir model, K_L represented the degree of adsorption affinity between the adsorbate and the adsorbent. The high enough K_L value for SPM/Hap indicated a strong affinity of Cu^{2+} (Table 3). Additionally, the adsorption capacities of Cu^{2+} ions removal by means of various adsorbents are presented in Table 4, which apparently confirms the higher potential of SPM/Hap to remove the Cu^{2+} from aqueous solutions.

3.4. Design of batch sorption from isotherm data

The schematic diagram of a batch sorption system is represented in Fig. 8. From this figure, it can be seen that the Cu^{2+} solution with the initial volume of (V) and the concentration of (C_o) reached equilibrium and declined to C_e .

During the batch adsorption system, desirable quantity (m) of SPM/Hap was poured into the solution and the amount of adsorbed metal ions were transformed from q_o to q_e . To find the mass balance, the following equation was used:

$$V(C_o - C_e) = m(q_o - q_e) \quad (10)$$

The obtained data of the adsorption experiments were followed closely by the Liu isotherm model. Consequently, the abovementioned equation (Eq. (8)) can be rearranged as follows:

$$\frac{m}{V} = \frac{C_o - C_e}{q_e} \Rightarrow m = \frac{(C_o - C_e)(1 + 3.2 C_e^{1.05}) V}{775.6 C_e^{1.05}} \quad (11)$$

Table 4

Comparison of maximum adsorption capacity (q_m) for Cu^{2+} with various adsorbents

Adsorbent	q_{\max} (mg g^{-1})	References
Chemically modified orange peel	15.27	[34]
Modified litchi pericarp	23.70	[7]
Activated carbon/chitosan composite	74.35	[35]
<i>Posidonia oceanica</i> biomass	76.92	[8]
Chitosan/clay/magnetite	14.3	[36]
Nano- Fe_3O_4	8.90	[27]
Nanohydroxyapatite/chitosan composite	26.11	[37]
Alginate-immobilized bentonite clay	131.6	[4]
EDTA functionalized Fe_3O_4	46.27	[26]
Magnetite nanorods	79.10	[38]
Hydroxyapatite	125	[39]
Ag/ZnO on glass (flower-like)	837.7	[40]
Activated biochar	222.2	[41]
Hardwood (jarrah) biochars	4.39	[42]
Mesoporous silica adsorbent (Fe-N,N-SBA15)	29.9	[43]
SPM/Hap	247.6	Present work

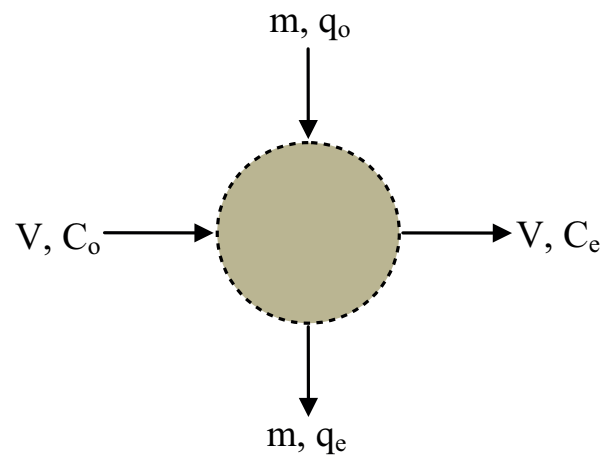


Fig. 8. Batch sorption process.

3.5. Application of SPM/Hap for removal of the Cu^{2+} from acid mine drainage

The adsorption study was conducted to evaluate the removal efficiency of Cu^{2+} from AMD by means of SPM/Hap as an adsorbent. In this regards, some samples containing 68.9 mg L^{-1} of Cu^{2+} were gathered from Sarcheshmeh Copper Complex wastewater (Kerman, Iran; see Supplementary Table 1). Afterwards, adsorption experiments were carried out in several plastic bottles containing a mixture of 50 mL

of AMD and 1.0 g L⁻¹ of adsorbent. The suspensions were then stirred vigorously at room temperature (25°C ± 1°C) and 150 rpm. The results of Cu²⁺ adsorption using SPM/Hap at both synthetic solution and AMD have been reported in Fig. 9. Accordingly, SPM/Hap represents a high capacity to adsorb Cu²⁺ onto the surfaces. Hence, it can be concluded that SPM/Hap is a cost-effective and promising adsorbent to remove Cu²⁺ from industrial wastewaters.

3.6. Desorption studies and reusability

Desorption experiments can be considered as an appropriate tool to recover the adsorbed metal ions from the adsorbent surfaces. Furthermore, it will enhance the reusability of the adsorbent to adsorb more metal ions and will also improve the sorption process [44].

$$\%DR = \frac{C_{des}}{C_{ads}} \times 100 \quad (12)$$

where %DR is the desorption ratio, C_{ads} is the amount of Cu²⁺ sorbed on the adsorbent, and C_{des} is the amount of Cu²⁺ desorbed from the adsorbent.

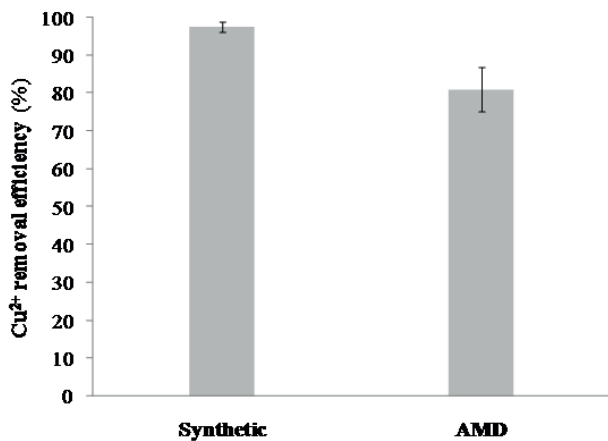


Fig. 9. Adsorptive removal efficiency of Cu²⁺ using SPM/Hap at synthetic and AMD solution (experimental conditions: solution pH 4.3 ± 0.1, adsorbent dose 1.0 g L⁻¹, reaction time 30 min, Cu²⁺ concentration 68.9 mg L⁻¹, and experimental temperature: 25°C ± 1°C).

Table 5

Repeated adsorption of Cu²⁺ ions using SPM/Hap nanoparticles (initial concentration 10 mg L⁻¹, SPM/Hap 1.0 g L⁻¹, contact time 60 min, 25°C ± 1°C)

Cycle number	pH 3.0		pH 5.0	
	Removal efficiency (%)	Desorption ratio (%)	Removal efficiency (%)	Desorption ratio (%)
1	94.5 (±2.3)	97.6 (±0.4)	99.9 (±0.0)	90.7 (±0.9)
2	90.8 (±1.9)	94.5 (±0.6)	98.7 (±0.4)	89.4 (±0.7)
3	85.0 (±0.5)	92.1 (±1.2)	94.5 (±0.5)	88.0 (±1.1)
4	81.1 (±1.3)	90.5 (±0.7)	91.1 (±0.6)	86.1 (±0.2)
5	77.5 (±0.8)	89.0 (±1.5)	89.9 (±0.2)	85.0 (±0.7)
Mean	85.8 (±6.9)	92.7 (±3.4)	94.8 (±4.4)	87.8 (±2.3)

Desorption experiments were performed in a batch system with Cu²⁺ solutions (50 mL, 10 mg L⁻¹) using 0.05 M EDTA solution as the eluent [21,45,46]. From Table 5, it can be seen that the adsorption/desorption experiments were carried out during five successive cycles and the removal efficiency of the adsorbent showed a slight decline (nearly 17% and 10% at pH 3.0 and 5.0, respectively) and still remained in the range of 77.5%–90% at the fifth cycle. Wholly, the ratio of Cu²⁺ desorption for pH 3.0 and 5.0 were over 92.7% (±3.4%) and 87.8% (±2.3%), respectively. In addition, numerous studies have reported large elution efficiency figures for several heavy metals, especially Cu²⁺, by means of EDTA as an eluent [46]. The findings of the desorption survey confirmed that no considerable loss could be observed in the performance of SPM/Hap nanoparticles over at least five cycles of adsorption/desorption, which proved the reusability of SPM/Hap nanoparticles in adsorbing heavy metals from contaminated waters.

4. Conclusions

Aiming at the removal of Cu²⁺ adsorptive from aqueous solutions, SPM/Hap nanoparticles were successfully synthesized, characterized and applied in a batch system. Considering the batch experiments, the sorption process of Cu²⁺ onto the surfaces of SPM/Hap seems to be a pH dependent process where the maximum amount of Cu²⁺ removal efficiency was obtained at pH 5.0–6.0. The surface complexation of SPM/Hap and ion exchange were found two most effective mechanisms involved in Cu²⁺ uptake from aqueous solution. Moreover, kinetic studies of the adsorption of Cu²⁺ onto the surfaces of SPM/Hap by means of various general kinetic models were investigated. The sorption seems to be governed by chemical forces rather than physical electrostatic interactions, possibly best described by the pseudo-first-order kinetic model, where the rate limiting step is assumed to be the chemical sorption between the adsorbate and the adsorbent. The results of equilibrium studies, in addition, show that the obtained data of Cu²⁺ adsorption were well described by both the Langmuir and Liu models with a high coefficient of correlation (R² = 0.996) and the sorption capacity of 247.6 mg g⁻¹. The desorption of Cu²⁺ together with the feasible recovery of SPM/Hap was performed by the application of EDTA as eluent with the high efficiency of 88%–93%. Ultimately, the results clearly indicated that the SPM/Hap

nanoparticles could be easily synthesized as a cost-effective, environmentally friendly, and robust adsorbent, and could be a very attractive candidate for the removal of toxic metals from waters and wastewaters.

Acknowledgments

The financial support of the Environmental Technologies Research Center (ETRC) and the Research and Technology Deputy of Ahvaz Jundishapur University of Medical Sciences (grant No.: ETRC9107) for this study are thankfully acknowledged.

References

- [1] A.R. Esfahani, A.F. Firouzi, G. Sayyad, A. Kiasat, L. Alidokht, A.R. Khataee, Pb(II) removal from aqueous solution by polyacrylic acid stabilized zero-valent iron nanoparticles: process optimization using response surface methodology, *Res. Chem. Intermed.*, 40 (2014) 431–445.
- [2] A. Esfahani, S. Hojati, A. Azimi, L. Alidokht, A. Khataee, M. Farzadian, Reductive removal of hexavalent chromium from aqueous solution using sepiolite-stabilized zero-valent iron nanoparticles: process optimization and kinetic studies, *Korean J. Chem. Eng.*, 31 (2014) 630–638.
- [3] A.A. Babaei, M. Bahrami, A. Farrokhian Firouzi, A. Ramazanpour Esfahani, L. Alidokht, Adsorption of cadmium onto modified nanosized magnetite: kinetic modeling, isotherm studies, and process optimization, *Desal. Wat. Treat.*, 56 (2015) 3380–3392.
- [4] W.S. Tan, A.S.Y. Ting, Alginate-immobilized bentonite clay: adsorption efficacy and reusability for Cu(II) removal from aqueous solution, *Bioresour. Technol.*, 160 (2014) 115–118.
- [5] A. Farrokhian Firouzi, A.A. Babaei, S. Hosseini, F. Heidarizadeh, Adsorption of copper(II) by modified magnetite nanoparticles: adsorption efficacy, equilibrium, kinetic and reusability, *Fresenius Environ. Bull.*, 24 (2015) 2815–2823.
- [6] N.-B. Chang, C. Houmann, K.-S. Lin, M. Wanielista, Fate and transport with material response characterization of green sorption media for copper removal via adsorption process, *Chemosphere*, 144 (2016) 1280–1289.
- [7] Z. Kong, X. Li, J. Tian, J. Yang, S. Sun, Comparative study on the adsorption capacity of raw and modified litchi pericarp for removing Cu(II) from solutions, *J. Environ. Manage.*, 134 (2014) 109–116.
- [8] Y. Hannachi, A. Rezugui, T. Boubaker, Biosorption potential of the mediterranean plant (*Posidonia oceanica*) for the removal of Cu²⁺ ions from aqueous media: equilibrium, kinetic, thermodynamic and mechanism analysis, *Korean J. Chem. Eng.*, 31 (2014) 1211–1218.
- [9] L.M. Fisher-Power, T. Cheng, Z.S. Rastghalam, Cu and Zn adsorption to a heterogeneous natural sediment: influence of leached cations and natural organic matter, *Chemosphere*, 144 (2016) 1973–1979.
- [10] D. Gusain, V. Srivastava, Y.C. Sharma, Kinetic and thermodynamic studies on the removal of Cu(II) ions from aqueous solutions by adsorption on modified sand, *J. Ind. Eng. Chem.*, 20 (2014) 841–847.
- [11] W.-S. Shin, K. Kang, Y.-K. Kim, Adsorption characteristics of multi-metal ions by red mud, zeolite, limestone, and oyster shell, *Environ. Eng. Res.*, 19 (2014) 15–22.
- [12] C.-G. Lee, J.-W. Jeon, M.-J. Hwang, K.-H. Ahn, C. Park, J.-W. Choi, S.-H. Lee, Lead and copper removal from aqueous solutions using carbon foam derived from phenol resin, *Chemosphere*, 130 (2015) 59–65.
- [13] X. Liang, Z. He, G. Wei, P. Liu, Y. Zhong, W. Tan, P. Du, J. Zhu, H. He, J. Zhang, The distinct effects of Mn substitution on the reactivity of magnetite in heterogeneous Fenton reaction and Pb(II) adsorption, *J. Colloid Interface Sci.*, 426 (2014) 181–189.
- [14] E. Gutiérrez-Segura, M. Solache-Ríos, A. Colín-Cruz, C. Fall, Comparison of cadmium adsorption by inorganic adsorbents in column systems, *Water Air Soil Pollut.*, 225 (2014) 1–13.
- [15] P. Xu, G.M. Zeng, D.L. Huang, C.L. Feng, S. Hu, M.H. Zhao, C. Lai, Z. Wei, C. Huang, G.X. Xie, Z.F. Liu, Use of iron oxide nanomaterials in wastewater treatment: a review, *Sci. Total Environ.*, 424 (2012) 1–10.
- [16] E. Skwarek, W. Janusz, D. Sternik, Adsorption of citrate ions on hydroxyapatite synthesized by various methods, *J. Radioanal. Nucl. Chem.*, 299 (2014) 2027–2036.
- [17] A. Salem, E. Velayi, Application of hydroxyapatite and cement kiln dust mixture in adsorption of lead ions from aqueous solution, *J. Ind. Eng. Chem.*, 18 (2012) 1216–1222.
- [18] A.A. Babaei, Z. Baboli, N. Jaafarzadeh, G. Goudarzi, M. Bahrami, M. Ahmadi, Synthesis, performance, and nonlinear modeling of modified nano-sized magnetite for removal of Cr(VI) from aqueous solutions, *Desal. Wat. Treat.*, 53 (2015) 768–777.
- [19] A.A. Babaei, M. Ahmadi, G. Goudarzi, N. Jaafarzadeh, Z. Baboli, Adsorption of chromium(VI) from saline wastewater using spent tea-supported magnetite nanoparticle, *Desal. Wat. Treat.*, 57 (2016) 12244–12256.
- [20] X. Hongqin, W. Duilin, J. Zhe, L. Xiaowei, Z. Shouwei, L. Yan, C. Cheng, Kinetic and thermodynamic sorption study of radiocobalt by magnetic hydroxyapatite nanoparticles, *J. Radioanal. Nucl. Chem.*, 292 (2012) 637–647.
- [21] Y. Feng, J.-L. Gong, G.-M. Zeng, Q.-Y. Niu, H.-Y. Zhang, C.-G. Niu, J.-H. Deng, M. Yan, Adsorption of Cd (II) and Zn (II) from aqueous solutions using magnetic hydroxyapatite nanoparticles as adsorbents, *Chem. Eng. J.*, 162 (2010) 487–494.
- [22] S. Zakhama, H. Dhaouadi, F. M'Henni, Nonlinear modelisation of heavy metal removal from aqueous solution using *Ulva lactuca* algae, *Bioresour. Technol.*, 102 (2011) 786–796.
- [23] S. Rangabhashiyam, N. Anu, M.S. Giri Nandagopal, N. Selvaraju, Relevance of isotherm models in biosorption of pollutants by agricultural byproducts, *J. Environ. Chem. Eng.*, 2 (2014) 398–414.
- [24] Z.-p. Yang, X.-y. Gong, C.-j. Zhang, Recyclable Fe₃O₄/hydroxyapatite composite nanoparticles for photocatalytic applications, *Chem. Eng. J.*, 165 (2010) 117–121.
- [25] S. Meski, S. Ziani, H. Khireddine, S. Boudboub, S. Zaidi, Factorial design analysis for sorption of zinc on hydroxyapatite, *J. Hazard. Mater.*, 186 (2011) 1007–1017.
- [26] Y. Liu, M. Chen, H. Yongmei, Study on the adsorption of Cu(II) by EDTA functionalized Fe₃O₄ magnetic nano-particles, *Chem. Eng. J.*, 218 (2012) 46–54.
- [27] X.S. Wang, L. Zhu, H.J. Lu, Surface chemical properties and adsorption of Cu (II) on nanoscale magnetite in aqueous solutions, *Desalination*, 276 (2011) 154–160.
- [28] R. Zhu, R. Yu, J. Yao, D. Mao, C. Xing, D. Wang, Removal of Cd²⁺ from aqueous solutions by hydroxyapatite, *Catal. Today*, 139 (2008) 94–99.
- [29] X. Xin, Q. Wei, J. Yang, L. Yan, R. Feng, G. Chen, B. Du, H. Li, Highly efficient removal of heavy metal ions by amine-functionalized mesoporous Fe₃O₄ nanoparticles, *Chem. Eng. J.*, 184 (2012) 132–140.
- [30] C. Yuan, C.-H. Hung, H.-W. Li, W.-H. Chang, Photodegradation of ibuprofen by TiO₂ co-doping with urea and functionalized CNT irradiated with visible light – effect of doping content and pH, *Chemosphere*, 155 (2016) 471–478.
- [31] F. Miyaji, Y. Kono, Y. Suyama, Formation and structure of zinc-substituted calcium hydroxyapatite, *Mater. Res. Bull.*, 40 (2005) 209–220.
- [32] M. Rafiee, M. Jahangiri-rad, Adsorption of reactive blue 19 from aqueous solution by carbon nano tubes: equilibrium, thermodynamics and kinetic studies, *Res. J. Environ. Sci.*, 8 (2014) 205–214.
- [33] L.D.T. Prola, E. Acayanka, E.C. Lima, C.S. Umpierrez, J.C.P. Vagheti, W.O. Santos, S. Laminsi, P.T. Djifon, Comparison of *Jatropha curcas* shells in natural form and treated by non-thermal plasma as biosorbents for removal of Reactive Red 120 textile dye from aqueous solution, *Ind. Crops Prod.*, 46 (2013) 328–340.

- [34] M.R. Lasheen, N.S. Ammar, H.S. Ibrahim, Adsorption/desorption of Cd(II), Cu(II) and Pb(II) using chemically modified orange peel: equilibrium and kinetic studies, *Solid State Sci.*, 14 (2012) 202–210.
- [35] Q. Liu, B. Yang, L. Zhang, R. Huang, Simultaneous adsorption of phenol and Cu²⁺ from aqueous solution by activated carbon/chitosan composite, *Korean J. Chem. Eng.*, 31 (2014) 1608–1615.
- [36] D.-W. Cho, B.-H. Jeon, C.-M. Chon, Y. Kim, F.W. Schwartz, E.-S. Lee, H. Song, A novel chitosan/clay/magnetite composite for adsorption of Cu(II) and As(V), *Chem. Eng. J.*, 200–202 (2012) 654–662.
- [37] M. Rajiv Gandhi, G.N. Kousalya, S. Meenakshi, Removal of copper(II) using chitin/chitosan nano-hydroxyapatite composite, *Int. J. Biol. Macromol.*, 48 (2011) 119–124.
- [38] H. Karami, Heavy metal removal from water by magnetite nanorods, *Chem. Eng. J.*, 219 (2013) 209–216.
- [39] S.T. Ramesh, N. Rameshbabu, R. Gandhimathi, P.V. Nidheesh, M. Srikanth Kumar, Kinetics and equilibrium studies for the removal of heavy metals in both single and binary systems using hydroxyapatite, *Appl. Water Sci.*, 2 (2012) 187–197.
- [40] S. Azizian, M. Bagheri, Enhanced adsorption of Cu²⁺ from aqueous solution by Ag doped nano-structured ZnO, *J. Mol. Liq.*, 196 (2014) 198–203.
- [41] L. Hadjittofi, M. Prodromou, I. Pashalidis, Activated biochar derived from cactus fibres – preparation, characterization and application on Cu(II) removal from aqueous solutions, *Bioresour. Technol.*, 159 (2014) 460–464.
- [42] S. Jiang, L. Huang, T.A.H. Nguyen, Y.S. Ok, V. Rudolph, H. Yang, D. Zhang, Copper and zinc adsorption by softwood and hardwood biochars under elevated sulphate-induced salinity and acidic pH conditions, *Chemosphere*, 142 (2016) 64–71.
- [43] Z. Zhang, H. Liu, L. Wu, H. Lan, J. Qu, Preparation of amino-Fe(III) functionalized mesoporous silica for synergistic adsorption of tetracycline and copper, *Chemosphere*, 138 (2015) 625–632.
- [44] A. El Nemr, Potential of pomegranate husk carbon for Cr(VI) removal from wastewater: kinetic and isotherm studies, *J. Hazard. Mater.*, 161 (2009) 132–141.
- [45] L. Dong, Z. Zhu, Y. Qiu, J. Zhao, Removal of lead from aqueous solution by hydroxyapatite/magnetite composite adsorbent, *Chem. Eng. J.*, 165 (2010) 827–834.
- [46] Y.-J. Wang, J.-H. Chen, Y.-X. Cui, S.-Q. Wang, D.-M. Zhou, Effects of low-molecular-weight organic acids on Cu(II) adsorption onto hydroxyapatite nanoparticles, *J. Hazard. Mater.*, 162 (2009) 1135–1140.

Supplementary information

Table S1
The characteristics of the acid mine drainage (AMD)

pH	EC ($\mu\text{S cm}^{-1}$)	Ca (mg L^{-1})	Mg (mg L^{-1})	Na (mg L^{-1})	SO_4^{2-} (mg L^{-1})	Fe (mg L^{-1})	Mn (mg L^{-1})	Cu (mg L^{-1})	Zn (mg L^{-1})	Al (mg L^{-1})	Ni (mg L^{-1})	Cd (mg L^{-1})
4.3	2,045	112	29.5	29.5	1,187	1.78	34.5	68.9	12.5	45.5	0.85	0.12

Table S2
Mathematical equations of the used isotherm and kinetic adsorption models

Model	Equation	Parameter and dimension
Isotherm models		
Langmuir	$q_e = \frac{K_L q_m C_e}{1 + K_L C_e}$	q_m (mg g^{-1}) K_L (L mg^{-1})
Freundlich	$q_e = K_F C_e^{\frac{1}{n}}$	K_F (mg g^{-1}) (mg L^{-1}) ⁻ⁿ n : model exponent
Redlich–Peterson	$q_e = \frac{K_{RP} C_e}{1 + a_{RP} C_e^g}$	K_{RP} (L g^{-1}) a_{RP} (L mg^{-1}) g ($0 < g < 1$)
Liu	$q_e = \frac{q_m (K_g C_e)^{n_L}}{1 + (K_g C_e)^{n_L}}$	K_g (L mg^{-1}) n_L
Kinetic models		
Pseudo-first-order (Lagergren)	$q_t = q_e (1 - \exp(-k_f t))$	k_f (min^{-1}) q_e, q_t (mg g^{-1})
Pseudo-second-order (Ho)	$q_t = \frac{k_s q_e^2 t}{1 + q_e k_s t}$	k_s ($\text{g mg}^{-1} \text{min}^{-1}$) t : time (min)
Elovich	$q_t = \left(\frac{1}{\beta}\right) \ln(1 + \alpha \beta t)$	α ($\text{mg g}^{-1} \text{min}^{-1}$) β (g mg^{-1})
Fractional power function	$q_t = a t^b$	a and b : model constants
Avrami fractional order	$q_t = q_e \{1 - \exp[-(k_{AV} t)]^{n_{AV}}\}$	k_{AV} (min^{-1}) n_{AV}
Intraparticle diffusion	$q_t = k_{id} t^{\frac{1}{2}} + C$	k_{id} : the intraparticle diffusion rate constant ($\text{mol g}^{-1} \text{min}^{-0.5}$).

Note: q_o is the maximum adsorption capacity (mg g^{-1}) and K_L is the adsorption equilibrium constant (L mg^{-1}). K_F and n are the adsorption capacity and the adsorption intensity, respectively. a_{RP} , K_{RP} and g are Redlich–Peterson constants, and the values of g lies between 0 and 1. For $g = 1$, R–P equation convert to Langmuir form. When a_{RP} and b_{RP} are much greater than unity, the equation can transform Freundlich form. Parameters k_f (min^{-1}) and k_s ($\text{mg g}^{-1} \text{min}^{-1}$) are rate coefficient for pseudo-first-order and pseudo-second-order kinetic models, respectively. α is the initial adsorption rate ($\text{mg g}^{-1} \text{min}^{-1}$) and β is the adsorption constant (g mg^{-1}). k_{AV} and n_{AV} are the Avrami rate constant (min^{-1}) and fractional reaction order (Avrami), respectively. k_{id} ($\text{mg g}^{-1} \text{min}^{-0.5}$) is the constant rate of intraparticle diffusion and C is the constant depicting the boundary layer effects. a ($\text{mg g}^{-1} \text{min}^{-b}$) and b are the fractional power kinetic model constants. q_e and q_t (mg g^{-1}) are adsorption capacity at equilibrium and at time t , respectively.

Table S3
List of coefficients of determination and error functions

Goodness of fit criteria	Abbreviation	Definition/expression
Determination coefficient	R^2	$R^2 = \frac{\sum_{i=1}^n (q_{i,\text{exp}} - \bar{q}_{i,\text{exp}})^2 - \sum_{i=1}^n (q_{i,\text{exp}} - q_{i,\text{calc}})^2}{\sum_{i=1}^n (q_{i,\text{exp}} - \bar{q}_{i,\text{exp}})^2}$
Adjusted determination coefficient	R^2_{adj}	$R^2_{\text{adj}} = 1 - (1 - R^2) \cdot \left(\frac{n-1}{n-p} \right)$
Sum squared error	SSE	$\text{SSE} = \sum_{i=1}^n (q_{i,\text{calc}} - q_{i,\text{exp}})^2$
Root mean square error	RMSE	$\text{RMSE} = \sqrt{\frac{\sum_{i=1}^n (q_{i,\text{exp}} - q_{i,\text{calc}})^2}{n}}$

Note: $q_{i,\text{calc}}$ is each value of q predicted by the fitted model, $q_{i,\text{exp}}$ is each value of q measured experimentally, $\bar{q}_{i,\text{calc}}$ is the average of $q_{i,\text{calc}}$, $\bar{q}_{i,\text{exp}}$ is the average of q measured experimentally, n is the number of experiments performed, and p is the number of parameters of the fitted model. The best model is the model with the lowest RMSE and SSE, as well as with R^2_{adj} and R^2 close to one.